Mon. Not. R. Astron. Soc. **331,** 521–536 (2002)

Modelling methanol and hydroxyl masers in star-forming regions

Dinah M. Cragg,[1★] Andrej M. Sobolev[2★] and Peter D. Godfrey[1★]
[1]*Department of Chemistry, Monash University, Clayton, Victoria 3800, Australia*
[2]*Astronomical Observatory, Ural State University, Lenin Street 51, Ekaterinburg 620083, Russia*

Accepted 2001 November 29. Received 2001 November 29; in original form 2001 October 12

ABSTRACT

Class II methanol masers are found in close association with OH main-line masers in many star-forming regions, where both are believed to flag the early stages in the evolution of a massive star. We have studied the formation of masers in methanol and OH under identical model conditions for the first time. Infrared pumping by radiation from warm dust at temperatures >100 K can account for the known maser lines in both molecules, many of which develop simultaneously under a range of conditions. The masers form most readily in cooler gas (<100 K) of moderately high density (10^5-10^8 cm^{-3}), although higher gas temperatures and/or lower densities are also compatible with maser action. The agreement between the current model (developed for methanol) and the established OH maser trends is very encouraging, and we anticipate that further tuning of the model will further improve such agreement.

We find the gas-phase molecular abundance to be the key determinant of observable maser activity for both molecules. Sources exhibiting both 6668-MHz methanol and 1665-MHz OH masers have a typical flux density ratio of 16; our model suggests that this may be a consequence of maser saturation. We find that the 1665-MHz maser approaches the saturated limit for OH abundances $>10^{-7.3}$, while the 6668-MHz maser requires a greater methanol abundance $>10^{-6}$. OH-favoured sources are likely to be less abundant in methanol, while methanol-favoured sources may be less abundant in OH or experiencing warm (>125 K), dense ($\sim 10^7$ cm^{-3}) conditions. These abundance requirements offer the possibility of tying the appearance of masers to the age of the new-born star via models of gas-phase chemical evolution following the evaporation of icy grain mantles.

Key words: masers – H II regions – ISM: molecules – radio lines: ISM.

1 INTRODUCTION

The earliest stages in the development of a massive star are hidden by the natal cloud of gas and dust which absorbs the young star's UV and visible emissions. The presence of a newly formed massive star can be inferred once it has generated an ultracompact region of ionized hydrogen (ucH II region), emitting a free–free radio continuum spectrum. Other indicators are infrared emission from dust which has been warmed by starlight, and molecular masers.

Masers of hydroxyl (OH), water (H_2O) and methanol (CH_3OH) occur in star-forming regions in close proximity to young massive stellar objects (see Caswell 2001b for a recent review). The 6668-MHz methanol maser, which has not been found in any other environment, is a useful tracer of early massive star formation, possibly preceding the development of detectable ucH II emission (Caswell 1996, 1997; Walsh et al. 1997, 1998; Codella & Moscadelli 2000; Minier, Conway & Booth 2001). The OH and H_2O masers are also detected in other environments, including late-type stars and as megamasers in external galaxies. In regions of high-mass star formation the methanol and OH masers are closely associated, for reasons which are the subject of this paper.

As well as providing signposts of recent massive star formation, the compact nature of masers can reveal details of the star-forming environment on a very fine scale. The water masers often display high velocities characteristic of outflows, while Zeeman splitting in the OH maser lines can probe local magnetic fields. As maser pumping requires specific conditions, modelling can provide estimates of the physical conditions in the maser regions, particularly where several transitions become masers simultaneously.

Methanol masers appear in certain microwave and millimetre transitions between adjacent K-ladders, in both the A and E symmetry species. Methanol masers are categorized as class I or class II, where each class pertains to a different set of transitions and a different maser environment (Menten 1991). Class I masers occur in star-forming regions, but are offset from IR and

★E-mail: Dinah.Cragg@sci.monash.edu.au (DMC); Andrej.Sobolev@usu.ru (AMS); Peter.Godfrey@sci.monash.edu.au (PDG)

radio-continuum sources and from other masers (Liechti & Wilson 1996). Some class I maser transitions show absorption at class II maser sites, and vice versa. Here we are concerned only with the class II masers, which are closely associated with sites of massive star formation, OH masers and ucH II emission. The strong 6- and 12-GHz class II methanol masers are accompanied in some sources by weaker masers in a variety of other methanol transitions. There is evidence that the masers at different frequencies may be coincident in velocity and/or position (e.g. Menten et al. 1988, 1992; Norris et al. 1993; Caswell et al. 1995b; Mehringer, Zhou & Dickel 1997; Moscadelli et al. 1999; Sutton et al. 2001).

Non-equilibrium population distributions including inversions are readily generated among the hyperfine levels of the low-lying rotational states in interstellar OH, giving rise to many maser lines. OH maser emission in regions of high-mass star formation is principally in the 1665-MHz main-line ground-state transition. Several other OH transitions commonly become masers in star-forming regions, with positional coincidence found in many cases (e.g. Caswell & Vaile 1995; Caswell 1998, 1999, 2001a; Desmurs et al. 1998; Gray et al. 2001). Other sources of OH maser emission, including late-type stars and supernova remnants, will not be discussed in detail here.

Many maser sources show emission at both OH and methanol frequencies, with high-resolution imaging showing that the maser spots from the two molecules are intermingled (e.g. Menten et al. 1992; Caswell, Vaile & Forster 1995c; Caswell 1997). Other sources show emission from one molecule only, and there is a range of behaviour between the methanol- and OH-favoured extremes (Caswell 1997). A key question is how the development of masers in one or both molecules is linked to the evolution of the new-born massive star, and to the emergence of a detectable ucH II region.

The evidence of coincidence between OH and methanol masers points to similar excitation conditions, and indeed IR pumping can account for both the OH (Guilloteau, Lucas & Omont 1981; Cesaroni & Walmsley 1991; Gray, Doel & Field 1991; Pavlakis & Kylafis 1996c; Gray 2001) and class II methanol masers (Cragg et al. 1992; Peng & Whiteoak 1993; Sobolev & Deguchi 1994a). In this paper we examine the maser pumping of both molecules under identical model conditions for the first time. Our maser model is described in Section 2. In Section 3 we present the results of calculations for both molecules over a range of conditions, and investigate whether a single model can account for all the observed masers. The model parameters which best account for the observations are summarized, and their implications discussed, in Section 4.

2 MASER MODELLING

Infrared pumping provides a mechanism for inverting the class II methanol masers. In the model of Sobolev & Deguchi (1994a, hereafter the SD model), methanol molecules are excited to the second and first torsionally excited states by radiation from warm dust. Masers appear in certain *b*-type transitions, following the radiative and collisional cascade back to the ground state. The maser brightnesses and flux ratios are affected by beaming, and by the amplification of background photons from an underlying ucH II region, although neither of these features is essential for the creation of population inversions. The model can account for the extreme brightness of observed 6- and 12-GHz masers (Sobolev, Cragg & Godfrey 1997a, hereafter SCG97a), and for the observation of weaker class II masers in many other methanol transitions (Sobolev, Cragg & Godfrey 1997b, hereafter SCG97b). The main-line masers in OH can also be inverted by IR pumping. The IR transitions connect hyperfine multiplets of different rotational levels, so they occur in groups which are closely spaced in frequency. It has long been known that line overlap can significantly influence the maser excitation in OH. Here we extend the SD model by including line overlap, and apply the same model to both methanol and OH.

The maser molecules are excited by radiation and collisions with hydrogen gas of density $n_{\rm H}$ and kinetic temperature $T_{\rm k}$. The large velocity gradient (LVG) approximation is used to evaluate the optical depth in the radiative transitions. An optical beaming factor is applied (Castor 1970), such that the optical depth in the line-of-sight direction is augmented by a beaming factor ϵ^{-1}, to simulate the extended geometry of the maser region. The optical depth is

$$\tau = \frac{hc}{4\pi}(N/\Delta V)\frac{(n_{\rm lo}/g_{\rm lo} - n_{\rm up}/g_{\rm up})g_{\rm up}B_{\rm Ein}}{1 + (\epsilon - 1)\cos^2(\theta)},$$

where θ is the angle between the considered ray and the line of sight, h is Planck's constant, c is the speed of light, n is the population and g the statistical weight of the level, and $B_{\rm Ein}$ is the Einstein coefficient for stimulated emission. The optical depth depends also the parameter $N/\Delta V$, where N is the column density of the maser molecule, and ΔV is the linewidth; this parameter is equivalent to the molecular volume density divided by the velocity gradient. $N/\Delta V$ is the specific column density perpendicular to the line of sight across the diameter D of the maser region. The optical depth in the line-of-sight direction is augmented by the beaming factor ϵ^{-1}, to simulate the extended geometry of the maser region. In the beamed or line-of-sight direction the maser path-length is effectively $L = \epsilon^{-1}D$, and the specific column density is effectively $\epsilon^{-1}N/\Delta V$.

The maser region is surrounded by a layer of warm dust at temperature $T_{\rm d}$, which provides the pumping photons, with dust filling factor $W_{\rm d}$ and dust optical depth $\tau_{\rm d} = \tau_{13}(\nu/10^{13})^2$ at frequency ν Hz. In our calculations $W_{\rm d} = 0.5$, $\tau_{13} = 1$, and usually $T_{\rm d} = 175$ K. In the majority of calculations described here the masers amplify continuum radiation from the 2.7-K microwave background alone. A few calculations also include an underlying ucH II region, where the masers are considered to be projected on the free–free continuum source. This H II continuum spectrum of temperature $T_{\rm e}[1 - \exp(-(f_{\rm e}/\nu)^2)]$ K is geometrically diluted by a factor $W_{\rm HII}$; here we use $T_{\rm e} = 10^4$ K and $f_{\rm e} = 1.2 \times 10^{10}$ Hz. The ucH II emission produces saturation effects in the masers, but for simplicity we include no special treatment of saturation. The model is based on a version of the LVG method for a uniform source, and includes only the saturation which is intrinsic to the basic multilevel LVG approach. The equations governing the SD model are set out in the appendix to SCG97a.

In the SD model the fractional abundance X of the maser molecule relative to hydrogen is obtained from the model parameters after assuming values for the velocity width ΔV and path-length L of the maser region along the line of sight: $X = (\epsilon^{-1} \times N/\Delta V \times \Delta V)/(n_{\rm H} \times L)$. Maser spots of both molecules are observed to be intermingled, and are typically clustered over an area of diameter 10^{17} cm (30 mpc or 1 arcsec at 6 kpc; Caswell 1997). It is reasonable to assume that the maser formation region is similarly extended in our direction, and we take the maser path-length to be $L = 10^{17}$ cm. We adopt beaming factor $\epsilon^{-1} = 10$. Maser linewidths ΔV are typically 0.1–3 km s^{-1}, and we use $\Delta V = 1$ km s^{-1}. The methanol calculations are carried out

independently for the A and E symmetry species with parameter $N_M/\Delta V$, so to evaluate the fractional abundance of methanol X_M we must also choose a value for the relative abundance of the two symmetry species [A]/[E]. If the methanol is formed at very low temperatures on grain surfaces, there will be a small excess of the A species (SCG97a), but here we assume the high-temperature equilibrium [A] = [E]. As an example, under these assumptions $N/\Delta V = 10^{12}\,\mathrm{cm^{-3}\,s}$ at hydrogen density $n_H = 10^7\,\mathrm{cm^{-3}}$ implies fractional abundances $X_{OH} = 10^{-6}$ for OH, and $X_M = 10^{-5.7}$ for methanol, after accounting for both symmetry species. A longer maser path or a smaller maser linewidth would generate smaller values of X.

Energy levels and line strengths for methanol were obtained from Mekhtiev, Godfrey & Hougen (1999). Exploratory calculations were carried out using the lowest 187 E-species and 190 A-species levels in the torsional ground state (up to $280\,\mathrm{cm^{-1}}$, $J_{max} = 18$), together with the corresponding levels in the first and second torsionally excited states, making 561 E-species and 570 A-species levels in total (up to $850\,\mathrm{cm^{-1}}$). The final calculations presented in the plots of maser brightness temperature were undertaken with 852 E-species and 861 A-species levels ($J_{max} = 22$). The results with the larger data set differ only slightly from those with the smaller set, with small differences apparent at $T_k > 100\,\mathrm{K}$ and for some predicted weak maser transitions involving $J > 10$. Thus the smaller data set does not contribute significant truncation errors at low temperatures, but may be inadequate at high temperatures. Calculations for OH were carried out using the lowest 48 energy levels (up to $825\,\mathrm{cm^{-1}}$, $J_{max} = 13/2$), obtained from Comben & Brown (1988). Line strengths for the microwave transitions were obtained from Destombes et al. (1977), and for the infrared transitions from Brown et al. (1982) and Goorvitch et al. (1992). Some calculations were repeated using 56 levels, with insignificant changes to the results.

There are no good estimates for the collisional transition rates for methanol. We used the model of Peng & Whiteoak (1993), based on the trends identified in double resonance experiments on E-species methanol by Lees & Haque (1974). For the A-species we adopted the same propensity rules, as described in SCG97a. The brightest methanol masers are not strongly influenced by the choice of collision model, as shown by previous calculations with non-selective collisions (SCG97a; SCG97b; Cragg et al. 2001). For OH the rate constants calculated by Offer, van Hemert & van Dishoeck (1994) were adopted. These rates were initially calculated for 28 levels, but have since been extended to 48 levels (A. R. Offer, unpublished calculations). We find that it is essential to include more than 28 levels to obtain reliable results for the $^2\Pi_{3/2}\,J = 5/2$ OH transitions at 6 GHz. The exact values of the collision rate constants adopted for the high-lying levels are not so important, however. We find very minor differences between maser calculations using the accurate rates for all 48 levels, and those using accurate rates for the lowest 28 levels together with approximate rates for levels 29–48, using extrapolation based on the trends identified by Offer et al.

Line overlap has been found to play an important role in the excitation of OH masers (e.g. Guilloteau et al. 1981; Cesaroni & Walmsley 1991; Gray et al. 1991; Pavlakis & Kylafis 1996a; Gray 2001). We have modified the SD model to include 'static cloud' local overlap, following the formalism of Guilloteau et al. (1981). We use a linewidth for overlap of $1\,\mathrm{km\,s^{-1}}$ in the calculations reported here. This ensures that the 1665-MHz transition is the dominant main-line OH maser, as observed in star-forming regions, whereas if line overlap is omitted we find the 1667-MHz maser to be stronger. Pavlakis & Kylafis (1996a,b,c, 2000) have undertaken a comprehensive investigation of the effects of both local and non-local overlap on OH masers. Our treatment of local overlap produces results qualitatively similar to those of Pavlakis & Kylafis (1996c), with $\Delta V = 1\,\mathrm{km\,s^{-1}}$ for the ground-state transitions. Previous investigations have suggested that line overlap does not produce a significant effect in methanol (SCG97a; Röllig et al. 1999), as our new calculations confirm. We find the effects of overlap to be significant only for a few predicted weak maser lines, in particular the $v_t = 1\ J_0 - J_1$ E series of lines at 189.7 GHz. The calculated brightness temperatures presented here include the effects of line overlap, but this can safely be omitted in future work on methanol, since its impact is negligible for the masers strong enough to be observed.

Our model differs from the recent treatment of OH masers by Pavlakis & Kylafis in the following respects: (1) we use 48 energy levels compared to their 28, (2) our dust spectrum has the form $W_d[1 - \exp(-\tau_d)]B(T_d)$ (where B is the Planck function), whereas theirs is $W(\nu/\nu_0)^p B(T_d)$; these behave differently at high frequencies, (3) our modelling differs in the angular distribution of the optical depth, and (4) we include only local line overlap, while they consider both local and non-local overlap. Despite these differences, the models are essentially similar, and we can compare results for warm gas ($T_k = 150\,\mathrm{K}$), warm dust ($T_d = 200\,\mathrm{K}$) calculations, although differences between the detailed treatment of optical depth, etc. in the two models remain. With a suitable choice of parameters, we obtain qualitatively similar results to those of Pavlakis & Kylafis (1996c) for $\Delta V = 1\,\mathrm{km\,s^{-1}}$; that is, we obtain masers at 1665, 1667 and 1720 MHz at low density and OH column density, replaced by masers at 1612 and 4765 MHz at high density and OH column density. Quantitative differences remain, due in part to differences between the models, but also due to truncation. We find that the model brightness temperatures for these five transitions are significantly affected if we reduce the number of levels in our calculations to 28. These differences are more pronounced for the $^2\Pi_{3/2}\,J = 5/2$ transitions at 6 GHz, where our results differ substantially from those of Pavlakis & Kylafis (2000). We see little evidence of the 6-GHz masers at such high gas temperatures (150 K) unless the number of energy levels is reduced to 28, which generates masers at 6031 and 6049 MHz in our calculations. We conclude that the results of Pavlakis & Kylafis (2000) for the 6-GHz OH masers are excessively affected by truncation. This is not unexpected, as truncation at 28 levels omits fast IR transitions into the $^2\Pi_{3/2}\,J = 5/2$ levels.

In the iterative solution of statistical equilibrium calculations, estimates of the level populations are used to evaluate the line optical depths, allowing improved estimates to be obtained by solving simultaneous linear equations for the level populations. This process is repeated until a satisfactory level of convergence is obtained. We find that the very different energy level schemes for methanol and OH require different convergence strategies. In methanol calculations the solution is typically obtained after steady convergence in a few hundred iterations, and convergence to one part in 10^3 is usually adequate. The methanol calculations require considerable computer time because of the large number of simultaneous equations to be solved. In OH calculations each iteration is accomplished much more quickly because there are fewer level populations to be obtained, but the solution typically requires some thousands of iterations and is oscillatory in nature, and convergence to one part in 10^4 or better is required to give a reproducible result. Despite the more stringent convergence requirements, calculations for OH are much faster overall. These

differences can be attributed to the effects of very similar competing processes populating the closely coupled energy levels in OH, whereas in methanol the upper and lower maser levels belong to different K-ladders and hence are independently populated by transitions with little in common.

The size of the maser spots must be estimated in order to compare the observed maser flux densities with the brightness temperatures of maser lines calculated from the model. VLBI estimates suggest typical maser spot sizes of a few milliarcsec ($<10^{15}$ cm at distance 6 kpc) (e.g. Reid et al. 1980; Menten et al. 1992; Moscadelli et al. 1999; Slysh et al. 2001). In this paper we look at the constraints placed on the physical parameters by the presence or absence of different masers, and whether observed combinations can be readily explained under plausible model conditions. This qualitative approach avoids the need for detailed assumptions about maser spot sizes, and we make quantitative estimates only for the ratio of intensities of the dominant methanol and OH masers.

3 RESULTS

We have examined the behaviour of the methanol and OH masers in the SD model as a function of four main parameters: the dust temperature T_d, the gas kinetic temperature T_k, the gas density n_H and the specific column density $N/\Delta V$ of the molecule of interest. Our calculations are usually performed as cuts through the four-dimensional parameter space along a single parameter axis. Each calculation starts from a previous nearby solution to speed convergence, and continuity provides a useful convergence check, especially when the same region of parameter space is traversed independently along different axes.

Selected calculation results are presented in Figs 1–7, in which the top panels display the behaviour of methanol maser transitions as the model parameters are varied, while the second panels display the OH masers. Note that we show only four of the many known methanol maser transitions, while the seven OH transitions shown include all the major observed and calculated masers. Observed

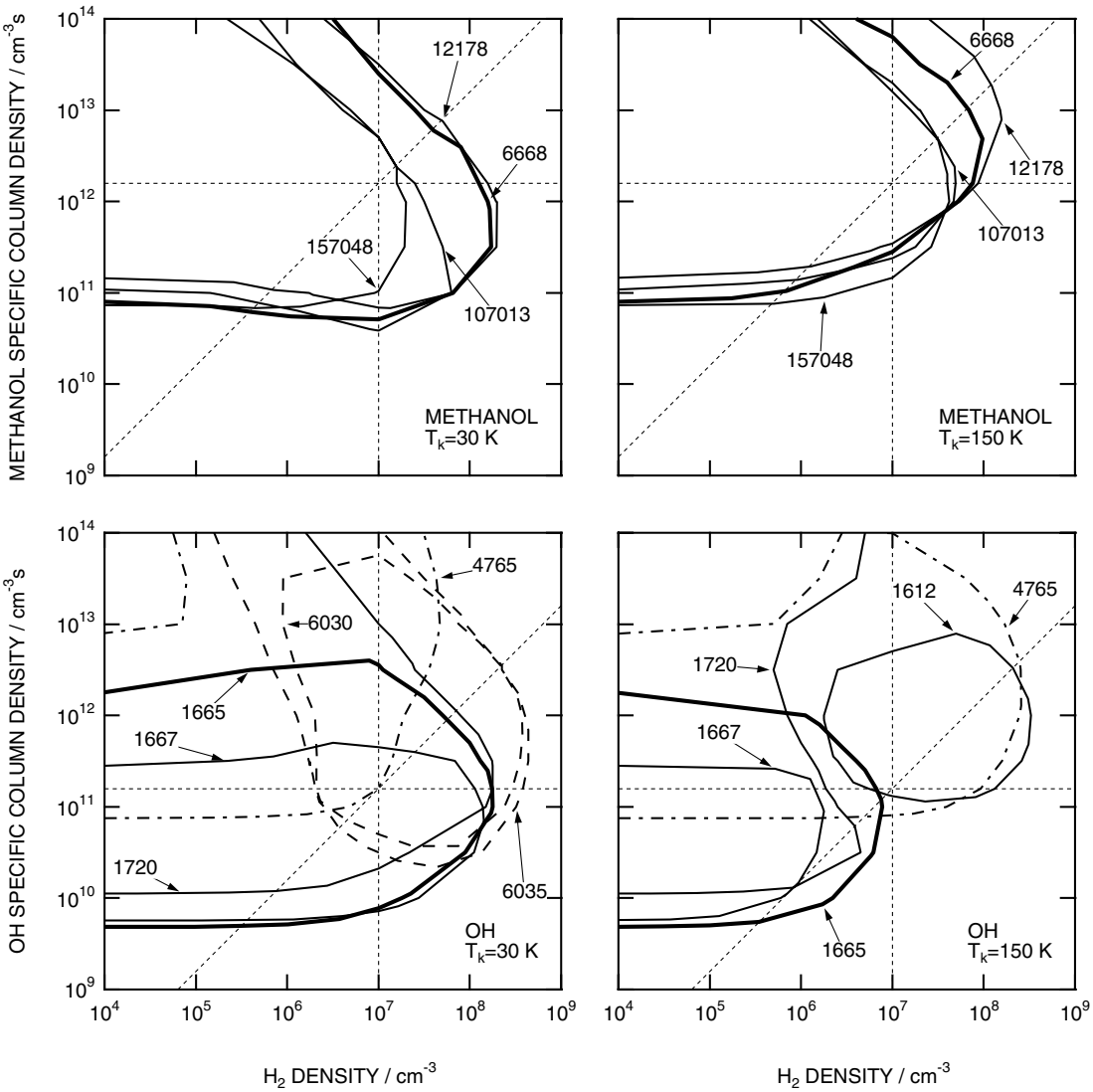

Figure 1. Contour diagram showing regions where selected masers of methanol and OH become active, as a function of hydrogen density n_H and specific column density of the maser molecule $N/\Delta V$, for $T_k = 30$ K (left-hand panels) and $T_k = 150$ K (right-hand panels). Contours are labelled with the line frequency in MHz. For each maser a single contour representing a brightness temperature of 10^4 K is drawn, with no masers appearing above this threshold in the bottom right regions of the plots. Dotted lines show the trajectories plotted in Figs 2–4, intersecting at the points common to all calculations in Figs 2–7. The remaining model parameters are fixed with values $T_d = 175$ K, $\epsilon^{-1} = 10$, and no ucH II background radiation.

trends and model results for individual maser transitions are discussed in Section 3.1 for methanol, and in Section 3.2 for OH. The bottom panels in Figs 2–7 show the ratio of brightness temperatures in the methanol 6668-MHz maser and the OH 1665-MHz maser (drawn as thick lines in the preceding panels), as discussed in Section 3.3. We compare the trends and patterns known from observations with the qualitative behaviour of the masers in our models, to obtain indications of values of the model parameters consistent with those trends, so delimiting the range of physical conditions likely to occur in maser formation regions.

Fig. 1 is a contour plot displaying the occurrence of masers as a function of two variables, the hydrogen density $n_{\rm H}$ and the specific column density of the maser molecule $N/\Delta V$. (Note that $N_{\rm M}/\Delta V$ is the parameter value for methanol A or E species, so the total specific column density of methanol is $2N_{\rm M}/\Delta V$.) Here the dust temperature is fixed at $T_{\rm d} = 175\,{\rm K}$ and two values of kinetic temperature are examined, with $T_{\rm k} = 30\,{\rm K}$ in the left-hand panels and $T_{\rm k} = 150\,{\rm K}$ in the right-hand panels. Each maser line is represented by a single contour, which delineates the area in which the maser brightness temperature $T_{\rm b}$ exceeds $10^4\,{\rm K}$. This threshold corresponds to flux density of 0.1 Jy for a 6-GHz maser of size 0.7 arcsec; maser spot sizes derived from VLBI observations are smaller than this, with inferred brightness temperatures correspondingly larger. Since the maser brightness temperatures rise and fall extremely rapidly (Figs 2 and 3), the position of the contours in Fig. 1 would not be greatly affected if the brightness temperature threshold were set at $10^6\,{\rm K}$ rather than $10^4\,{\rm K}$. As well as displaying the parameter ranges for which different maser transitions coincide, such a plot helps to clarify which features are brought about by collisions (governed by hydrogen density) and which are a result of optical depth (governed by specific column density of the maser molecule). Masers generally appear in the lower density region of the contour plot, while they switch off at high values of $n_{\rm H}$. The masers fall below our intensity threshold at low values of $N/\Delta V$ because of insufficient maser optical depth, while large optical depths in the pumping lines at high values of $N/\Delta V$ prevent pumping radiation from effectively penetrating the maser formation region. Other processes influence the high $N/\Delta V$

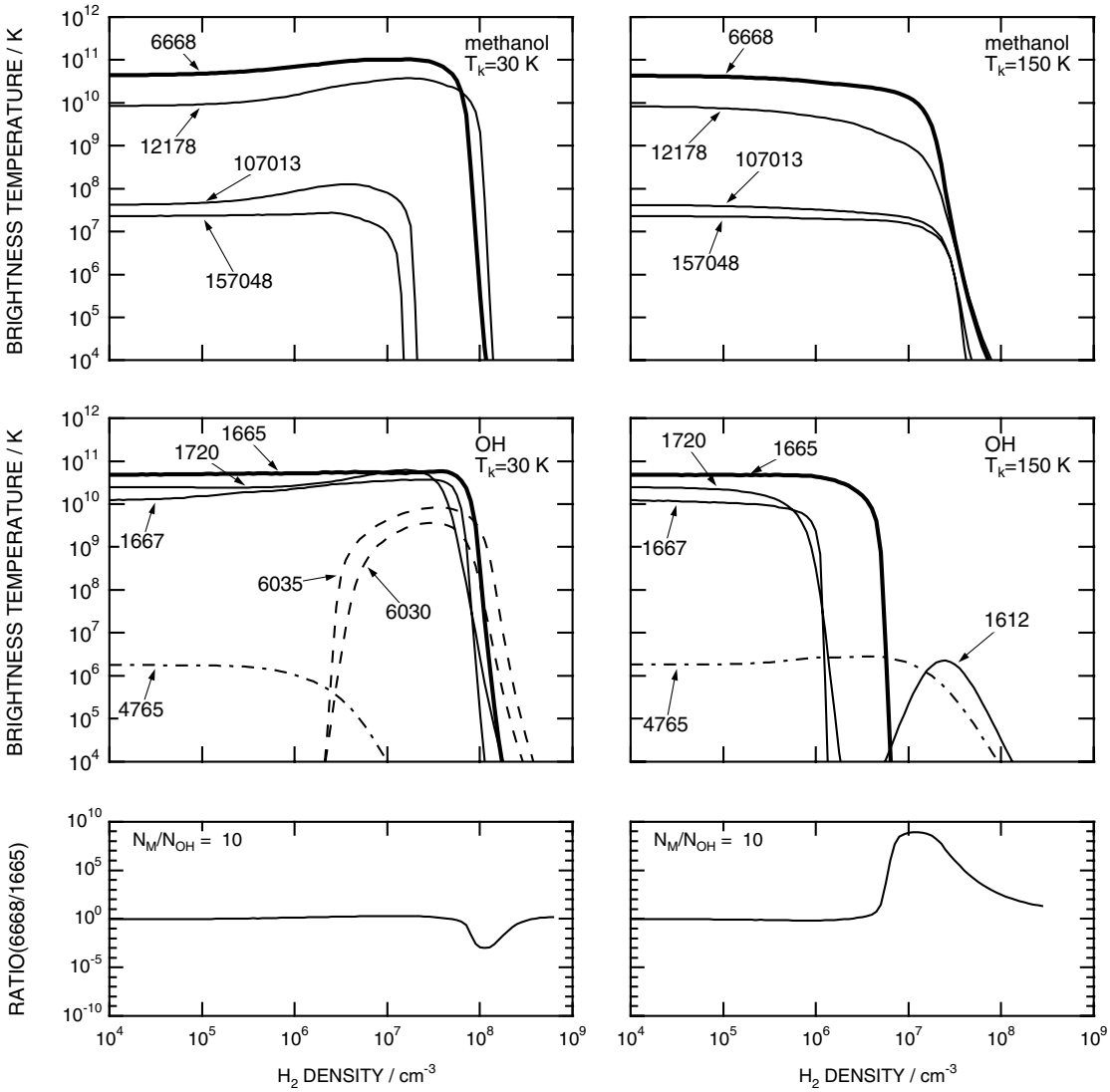

Figure 2. Brightness temperatures for selected masers of methanol (top panels) and OH (middle panels) versus hydrogen density $n_{\rm H}$, for $T_{\rm k} = 30\,{\rm K}$ (left-hand panels) and $T_{\rm k} = 150\,{\rm K}$ (right-hand panels). The remaining model parameters are fixed with values $T_{\rm d} = 175\,{\rm K}$, $N_{\rm M}/\Delta V = 10^{12.2}\,{\rm cm^{-3}\,s}$, $N_{\rm OH}/\Delta V = 10^{11.2}\,{\rm cm^{-3}\,s}$, $\epsilon^{-1} = 10$, and no ucH II background radiation. Bottom panels show ratio of brightness temperatures for methanol 6668-MHz and OH 1665-MHz lines.

boundary as well, the most important of which are competitions between different maser transitions (see Field & Gray 1988; Gray, Field & Doel 1992 or Sobolev & Deguchi 1994b). Our results are least reliable in the upper left regions of the plots in Fig. 1, where the LVG treatment of the saturated limit is likely to be inadequate.

Figs 2–4 show the behaviour of the masers along three axes through a single point in each of the four plots in Fig. 1. The point chosen is $n_{\rm H} = 10^7\,{\rm cm}^{-3}$ with $N_{\rm M}/\Delta V = 10^{12.2}\,{\rm cm}^{-3}\,{\rm s}$ for methanol and $N_{\rm OH}/\Delta V = 10^{11.2}\,{\rm cm}^{-3}\,{\rm s}$ for OH, with $T_{\rm d} = 175\,{\rm K}$ and $T_{\rm k} = 30$ and $150\,{\rm K}$ as before. This choice was made to illustrate the different maser regimes in OH. Fig. 2 shows hydrogen density variation (horizontal trace in Fig. 1), while Fig. 3 shows specific column density variation (vertical trace in Fig. 1). Fig. 4 shows a series of calculations at fixed fractional abundance X of the maser molecule relative to hydrogen, represented by the diagonal trace in Fig. 1. Both the hydrogen density (bottom axis) and the column density of the maser molecule (top axis) change along the trajectory in Fig. 4. Note that points above the diagonal in Fig. 1 represent either very large abundances of the maser molecule relative to hydrogen, or very long maser path-lengths (see below), so the fixed X trajectory samples a range of plausible maser model conditions, while the horizontal and vertical trajectories extend to the extremes. Fig. 5 shows the maser dependence on dust temperature $T_{\rm d}$ through the common points, while Fig. 6 shows the dependence on gas kinetic temperature $T_{\rm k}$. Fig. 7 shows the effect of adding an underlying ucH II region to the background continuum, as discussed in Section 3.4.

It is apparent from Figs 1 and 3 that the minimum specific column density of methanol required to produce strong masers is greater than that required of OH by approximately an order of magnitude ($N_{\rm M}/\Delta V > 10^{10.7}\,{\rm cm}^{-3}\,{\rm s}$, $N_{\rm OH}/\Delta V > 10^{9.7}\,{\rm cm}^{-3}\,{\rm s}$). If the methanol and OH masers both develop over a maser path of 10^{17} cm and have velocity width $\Delta V = 1\,{\rm km\,s}^{-1}$, then the minimum values of fractional abundance which lead to masers with

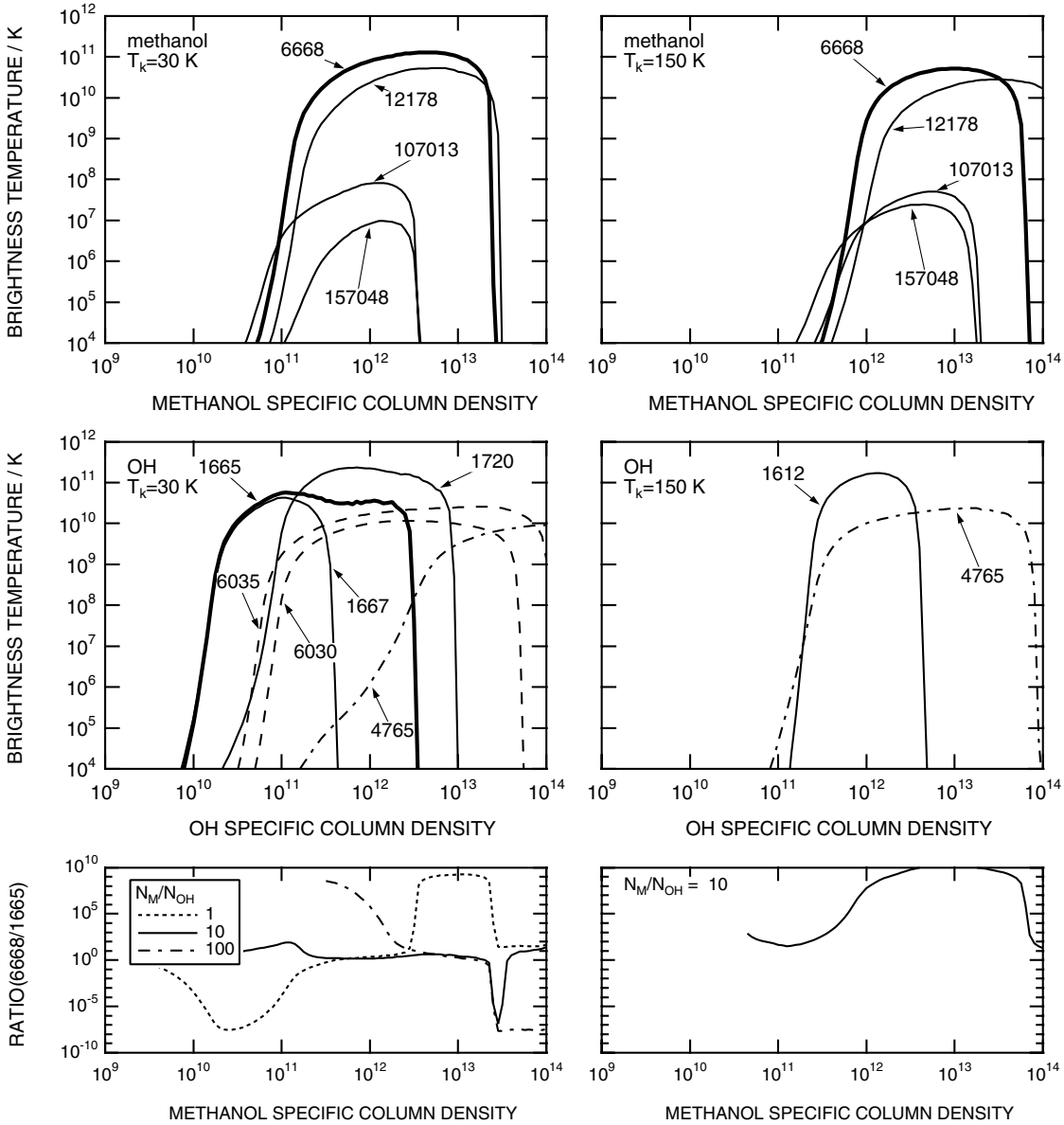

Figure 3. Brightness temperatures for selected masers of methanol and OH versus specific column density $N/\Delta V$, for $T_{\rm k} = 30\,{\rm K}$ and $T_{\rm k} = 150\,{\rm K}$. The remaining model parameters are fixed with values $n_{\rm H} = 10^7\,{\rm cm}^{-3}$, $T_{\rm d} = 175\,{\rm K}$, $\epsilon^{-1} = 10$, and no ucH II background radiation. Bottom panels show ratio of brightness temperatures for methanol 6668-MHz and OH 1665-MHz lines.

brightness temperatures $T_b > 10^4$ K are $X_M = 10^{-7.5}$ for methanol and $X_{OH} = 10^{-8.5}$ for OH (at low gas temperatures). Under the same assumptions the diagonal trajectories illustrated in Figs 1 and 4 represent $X_M = 10^{-5.5}$ for methanol and $X_{OH} = 10^{-6.8}$ for OH, after accounting for the A and E methanol symmetry species and the beaming factor $\epsilon^{-1} = 10$.

In star-forming regions where masers of both molecules are observed, each must be above its respective threshold. The minimum methanol abundance required for observable masers is greater than the OH minimum; if both molecules are present with $X > 10^{-7.5}$, then masers of both types should be observable under appropriate pumping conditions. Both molecules are thought to be enriched in the gas phase in star-forming regions, following the evaporation of icy grain-mantles (Hartquist et al. 1995), and each may perhaps attain an abundance as large as $X = 10^{-5}$. In comparing the masers of OH and methanol under common model conditions we must assume a value for their relative abundance N_M/N_{OH}. We find the greatest common ground in the conditions producing masers in the two molecules when the methanol abundance is greater with $N_M/N_{OH} = 10$, as illustrated in Figs 2–7. These points are discussed further in Section 3.3.

When the dust continuum temperature is low enough that only

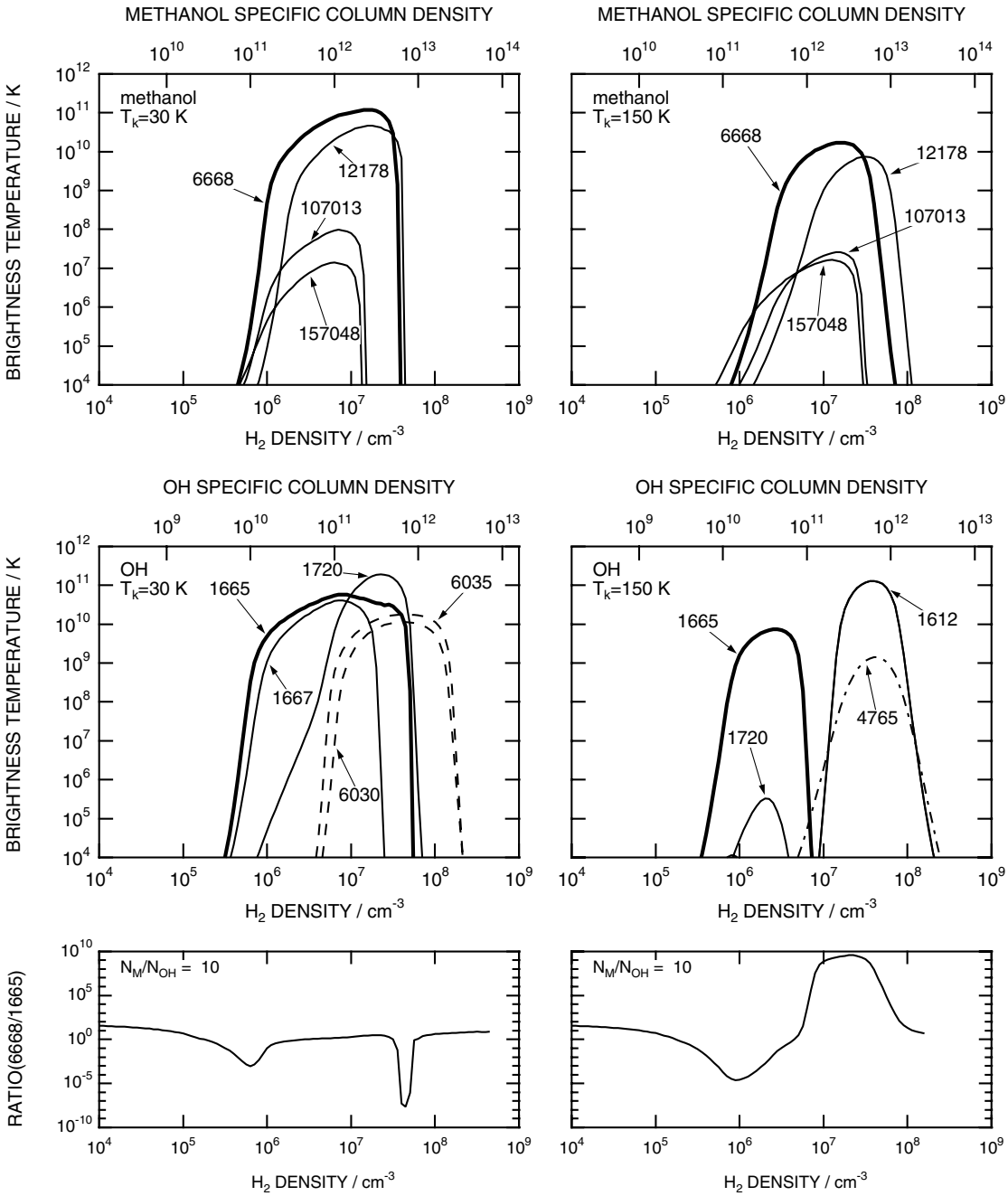

Figure 4. Brightness temperatures for selected masers of methanol and OH with fixed fractional abundance X relative to hydrogen, for $T_k = 30$ K and $T_k = 150$ K. Under the assumptions outlined in Section 2 these plots represent $X_M = 10^{-5.5}$ for methanol and $X_{OH} = 10^{-6.8}$ for OH. The bottom axis shows hydrogen density n_H, while the top axis shows specific column density $N/\Delta V$ of the maser molecule. The remaining model parameters are fixed with values $T_d = 175$ K, $\epsilon^{-1} = 10$, and no ucH II background radiation. Bottom panels show ratio of brightness temperatures for methanol 6668-MHz and OH 1665-MHz lines.

ground-state methanol levels are significantly populated ($T_d < 50$ K), the masers switch from class I to class II behaviour as the gas temperature T_k is varied, with the class I masers appearing when $T_d < T_k$ and the class II masers when $T_d > T_k$ (Cragg et al. 1992). In contrast, in the calculations reported here the dust temperature and the methanol column density are both high enough to promote the class II masers throughout the range of parameters examined, although the masers are diminished in brightness when $T_d < T_k$. Fig. 1 shows a single regime of methanol maser activity over which the four selected transitions become masers simultaneously, although the millimetre masers exceed our threshold over a narrower range of conditions. Some of the other weaker maser transitions are more sensitive to the choice of parameters and delineate a specific range of density or temperature, so they can provide useful constraints in multi-transition modelling (Cragg et al. 2001; Sutton et al. 2001).

The OH maser transitions illustrated show a more complex pattern of behaviour, with the ground-state main-line masers switching off when the gas density, gas temperature and OH column density are all high, to be replaced by the 1612-MHz satellite line maser. (Elitzur 1982 describes the competing radiative processes which can lead to either 1612-MHz satellite or main-line masers in the context of IR pumping of masers in late-type stars.) Furthermore, at low gas temperatures the excited-state 6035- and 6031-MHz masers (shown as dashed lines) appear only at high gas density and OH column density. The common point through which all trajectories in Figs 2–7 pass is chosen to sample this high-density, high-column-density region, so that the changeover from one regime of behaviour to another can be illustrated. Note that these different regimes of behaviour do not appear for all parameter choices, e.g., at lower values of hydrogen density $n_H < 10^6$ cm^{-3}.

3.1 Results of methanol calculations

Approximately 20 different class II methanol maser transitions have been observed in star-forming regions. Calculations with the SD model for a variety of parameter combinations can account for the presence of masers in all these lines (SCG97b), and suggest a large number of other potential maser candidate transitions, particularly under conditions of low gas temperature. In Figs 1–7

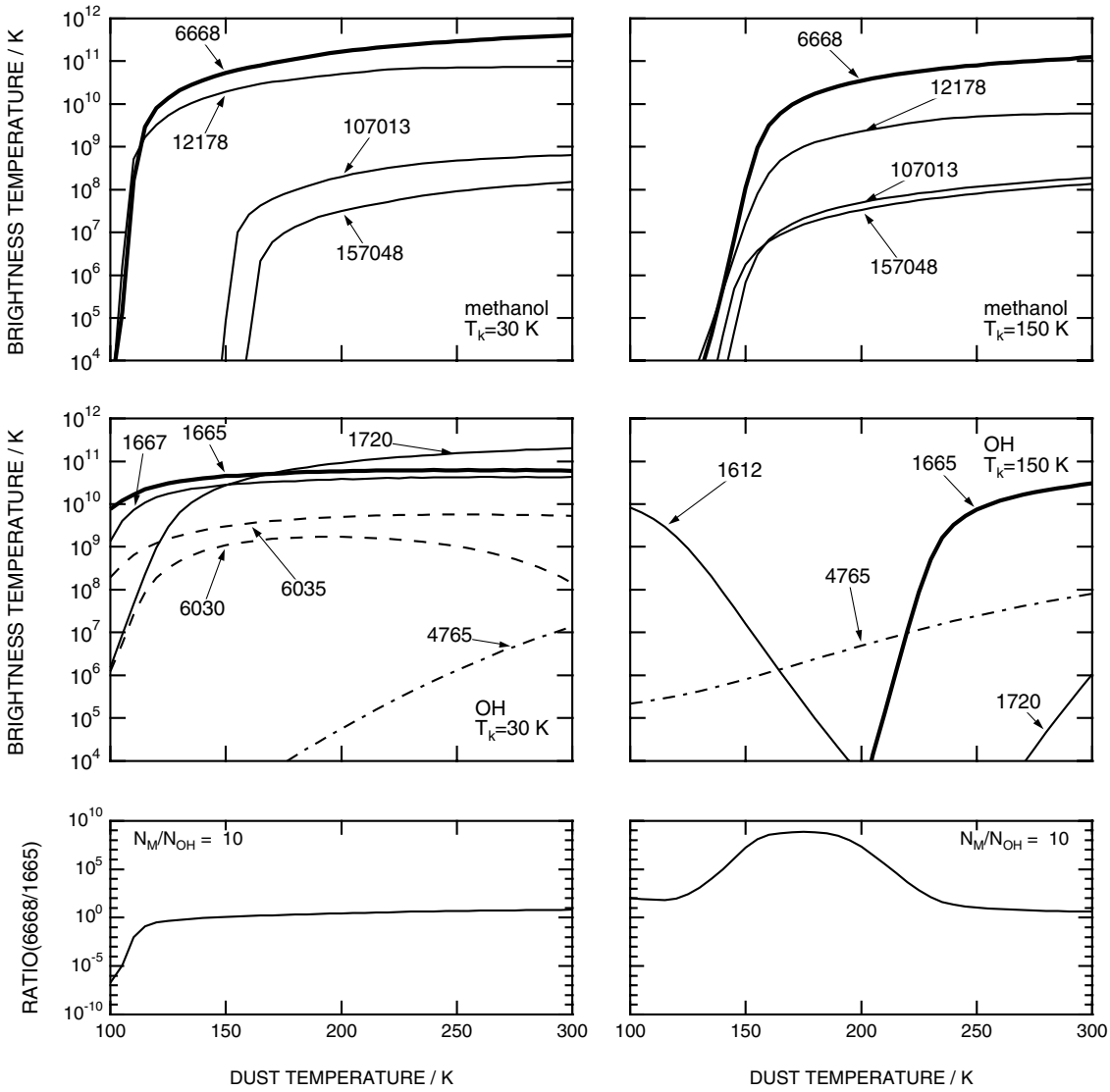

Figure 5. Brightness temperatures for selected masers of methanol and OH versus dust temperature T_d, for $T_k = 30$ K and $T_k = 150$ K. The remaining model parameters are fixed with values $n_H = 10^7$ cm^{-3}, $N_M/\Delta V = 10^{12.2}$ cm^{-3} s, $N_{OH}/\Delta V = 10^{11.2}$ cm^{-3} s, $\epsilon^{-1} = 10$, and no ucH II background radiation. Bottom panels show ratio of brightness temperatures for methanol 6668-MHz and OH 1665-MHz lines.

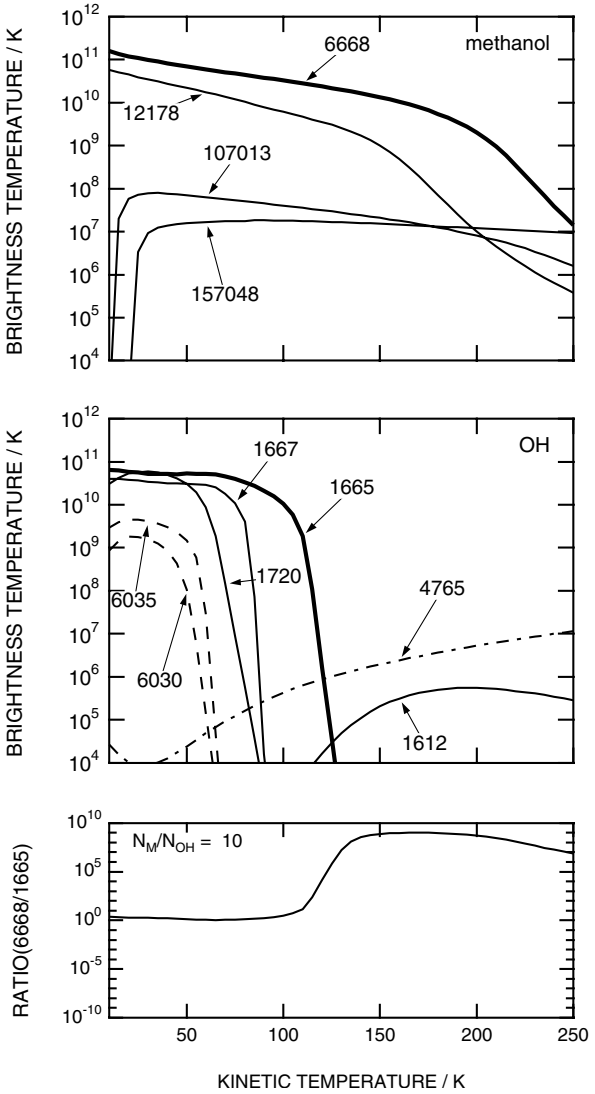

Figure 6. Brightness temperatures for selected masers of methanol and OH versus kinetic temperature T_k. The remaining model parameters are fixed with values $n_H = 10^7\,cm^{-3}$, $T_d = 175\,K$, $N_M/\Delta V = 10^{12.2}\,cm^{-3}\,s$, $N_{OH}/\Delta V = 10^{11.2}\,cm^{-3}\,s$, $\epsilon^{-1} = 10$, and no ucH II background radiation. The bottom panel shows the ratio of brightness temperatures for methanol 6668-MHz and OH 1665-MHz lines.

(top panels) we illustrate only the four methanol maser transitions that have been widely surveyed in star-forming regions. Trends identified from these observations are summarized below for each transition in turn, followed by the modelling results. Some other transitions show more specific parameter requirements, and it would be useful if these were also surveyed more widely.

6668-MHz 5_1–6_0A^+ maser: The 6668-MHz transition is the strongest and most widespread methanol maser, with brightness temperature exceeding $3 \times 10^{12}\,K$ in W3(OH) (Menten et al. 1992). It has already been detected at several hundred sites (Caswell et al. 1995a), while an unbiased survey suggests that there may be as many as 500 detectable sources in the Galaxy (Ellingsen et al. 1996). It is accompanied by ucH II continuum emission in less than half the sites investigated (Caswell et al. 1995a; Caswell 1996; Ellingsen et al. 1996). At the remaining sites it is still thought to be an indicator of massive star formation, possibly at a very early or deeply embedded stage.

In our calculations the 6-GHz maser is also the brightest methanol maser line under nearly all circumstances (Figs 2–7). Under the model conditions illustrated the 6-GHz maser appears at dust temperature $T_d > 100\,K$, but diminishes when the gas temperature T_k approaches or exceeds the dust temperature (Figs 5 and 6). This maser switches on for methanol specific column density $N_M/\Delta V > 10^{10.7}\,cm^{-3}\,s$, and attains peak brightness temperature $T_b \sim 10^{11}\,K$ (Fig. 3). The maser is excited at low gas density, and is independent of gas density up to $n_H \sim 10^8\,cm^{-3}$, where its brightness falls abruptly (Fig. 2). This indicates that the maser excitation mechanism is predominantly radiative, with collisional quenching at high density. For plausible values of methanol fractional abundance, $10^{-7.5} < X_M < 10^{-5}$, the bright 6668-MHz maser is restricted to the hydrogen density range $10^5 < n_H < 10^{8.3}\,cm^{-3}$ and methanol specific column density range $10^{10.7} < N_M/\Delta V < 10^{13.3}\,cm^{-3}\,s$, setting some constraints on the conditions in the maser regions.

12178-MHz 2_0–$3_{-1}E$ maser: The second strongest class II methanol maser, in both observations and modelling, is at 12178 MHz. This maser accompanies the 6-GHz maser at more than half the sites studied (Caswell et al. 1995b), and is also seen in a small number of sources in which the 6-GHz maser is not observed. It is generally weaker, typically by a factor of 10 in flux density, but stronger by up to a factor of 2.5 at some sites (Caswell et al. 1995b). High-resolution observations show excellent positional coincidence for the two transitions (Menten et al. 1992; Norris et al. 1993).

The model calculations, in which the 12-GHz excitation closely follows that at 6 GHz with peak brightness temperatures typically a little lower, are in accord with these observations. This maser requires a slightly higher column density of methanol to switch on, and also extends to slightly higher values of hydrogen density. Many of the sites in which only 6-GHz emission is known may have corresponding 12-GHz emission below the detection limit. The remaining sources displaying emission from only one of these transitions can be explained as examples at the extremes of the density or methanol abundance range (Fig. 4). The relative brightness of the 6- and 12-GHz masers is also sensitive to maser geometry as determined by the beaming factor (SCG97b).

107013-MHz 3_1–4_0A^+ maser: The 107-GHz methanol maser has been widely surveyed in southern class II methanol sources, with masers detected in 25 sources (Val'tts et al. 1995; Caswell et al. 2000). Flux densities are typically lower than at 6 GHz by a factor of 77 (Caswell et al. 2000). The presence of thermal emission in this transition at some maser sites can make it more difficult to distinguish weak maser emission. Coincidence between the 107- and 12-GHz masers in Cep A was established to arcsec accuracy by Mehringer et al. (1997), while coincidence of the 6-, 12-, 86- and 107-GHz methanol masers in W3(OH) within 2 arcsec was found by Sutton et al. (2001).

In our calculations the 107-GHz maser follows a similar pattern to the 6- and 12-GHz masers but at brightness temperatures lower by 3–4 orders of magnitude. This maser is usually quenched at lower density (Figs 1 and 2) and requires a higher dust temperature ($T_d > 150\,K$ at $T_k = 30\,K$) to turn on. The lower peak brightness temperature and more restricted range of parameters are consistent with the observation of this maser in a subset of 6-GHz sources.

157048-MHz 6_0–$6_{-1}E$ maser: The $J_0 - J_{-1}$ E methanol transitions fall in a group near 157 GHz, of which eight members have been identified as class II masers (Slysh, Kalenskii & Val'tts 1995). The $J = 6$ transition at 157048 MHz is among the strongest, while thermal emission in this line is also widespread (Slysh et al.

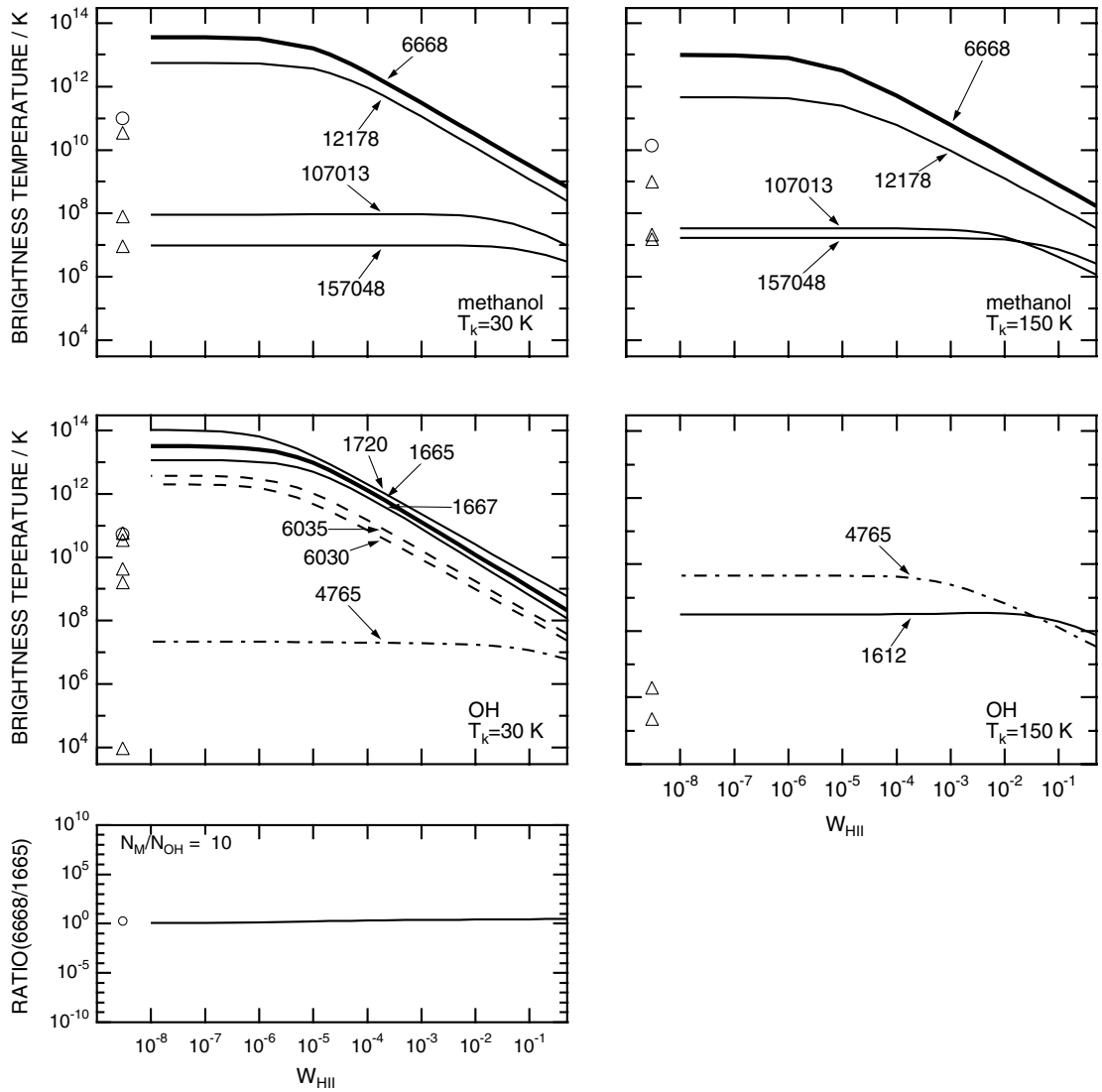

Figure 7. Brightness temperatures for selected masers of methanol and OH versus H II region dilution factor $W_{\rm HII}$, for $T_{\rm k} = 30$ K and $T_{\rm k} = 150$ K. Symbols represent results when no ucH II background radiation is included (circles are 6668-MHz methanol and 1665-MHz OH transitions, and triangles show remaining transitions which appear in the same sequence as the labelled curves). All other model parameters are fixed with values $n_{\rm H} = 10^7$ cm^{-3}, $T_{\rm d} = 175$ K, $N_{\rm M}/\Delta V = 10^{12.2}$ cm^{-3} s, $N_{\rm OH}/\Delta V = 10^{11.2}$ cm^{-3} s, $\epsilon^{-1} = 10$. The bottom panel shows ratio of brightness temperatures for methanol 6668-MHz and OH 1665-MHz lines at $T_{\rm k} = 30$ K; at $T_{\rm k} = 150$ K the 1665-MHz OH line is in absorption against the H II background.

1999). This maser is rarer than the 107-GHz maser, but is found in some of the same sources.

Our calculations show that the excitation of the selected 157-GHz maser line closely resembles that of the 107-GHz maser at high gas temperatures, but it is weaker by an order of magnitude at lower gas temperatures. These results suggest that the ratio of fluxes in the 107- and 157-GHz masers is likely to be a useful indicator of gas kinetic temperature.

3.2 Results of OH calculations

In Figs 1–7 we illustrate the seven OH maser transitions which have been widely surveyed in star-forming regions. These are also the dominant transitions in our maser modelling. We show the ground-state masers as solid lines (with the 1665-MHz maser emphasized), the excited state $^2\Pi_{3/2}$ masers as dashed lines, and the single $^2\Pi_{1/2}$ maser as a dot-dashed line. The most significant calculated masers omitted from these plots are the $^2\Pi_{3/2}$ $J = 7/2$ main-line transitions at 13441 and 13434 MHz, which appear in the low-temperature, high-density, high OH column density regime, with peak brightness temperature $\sim 10^6$ K in the trajectory in Fig. 4. Many of the OH maser lines have been systematically observed in surveys with a common sensitivity limit, providing good statistics from a near-complete sample of sources. The pattern of occurrence of these OH masers, summarized below for each transition in turn, is thus much better known than for the various methanol masers.

1665-MHz $^2\Pi_{3/2}$ $J = 3/2$ $F = 1 - 1$ maser: Approximately 200 sources of OH maser emission in star-forming regions are known (Caswell & Haynes 1987, and references therein; Caswell 1998), with the strongest OH emission at 1665 MHz in all but a few. A brightness temperature exceeding 6×10^{12} K has been estimated for the 1665-MHz main-line maser OH34.26+0.15 (Slysh et al. 2001).

We find the 1665-MHz maser to be the dominant maser in our calculations so long as the effects of line overlap are included in the modelling. In the SD model 1665-MHz OH maser emission

appears for gas temperatures $T_k < 125$ K under the conditions illustrated, with peak brightness $T_b \sim 10^{11}$ K. At low gas temperature ($T_k = 30$ K) the maser brightness is independent of density for $n_H < 10^8$ cm^{-3} (Fig. 2), indicating that this maser is also radiative in origin and collisionally quenched. Bright masers require an OH specific column density in the range $10^{9.7} < N_{OH}/\Delta V < 10^{12.7}$ cm^{-3} s and a hydrogen density $10^4 < n_H < 10^{8.3}$ cm^{-3} for plausible values of the OH fractional abundance, $10^{-8.5} < X_{OH} < 10^{-5}$. At low gas temperature the maser is independent of dust temperature in the range examined ($T_d = 100$–300 K), while at high gas temperature ($T_k = 150$ K) the 1665-MHz maser is present only for high dust temperatures $T_d > 200$ K or low gas densities $n_H < 10^7$ cm^{-3}.

1667-MHz $^2\Pi_{3/2}$ J = 3/2 F = 2–2 maser: While the 1665-MHz maser usually displays the strongest OH emission in star-forming regions, it is accompanied at 90 per cent of sites by 1667-MHz emission in the other main-line ground-state transition (Caswell & Haynes 1983). This is typically weaker by a factor of 3, but occasionally stronger by up to a factor of 4 (Caswell & Haynes 1987). High-resolution observations show the 1665- and 1667-MHz maser spots to be intermingled on the arcsecond scale (Caswell 1998; Argon, Reid & Menten 2000).

In our calculations the 1667-MHz maser accompanies the 1665-MHz maser at low gas temperatures, with slightly lower brightness temperature. At higher gas temperatures the 1667-MHz maser appears over a more restricted range of density ($n_H < 10^6$ cm^{-3}) (Fig. 1), and requires a much higher dust temperature ($T_d > 300$ K) to become excited at $n_H = 10^7$ cm^{-3}. This is consistent with it being quenched at lower kinetic temperatures ($T_k > 100$ K) than the 1665-MHz line, as shown in Fig. 6. The similarity between the two main-line masers in our calculations is in accord with the observations, as is the dominance of the 1665-MHz maser. In our calculations the 1667-MHz maser disappears at $N_{OH}/\Delta V > 10^{11.7}$ cm^{-3} s (Fig. 1). If confirmed by a better treatment of maser saturation, this would set a useful upper limit on OH column density for the great majority of OH maser sites.

1720-MHz $^2\Pi_{3/2}$ J = 3/2 F = 2 − 1 maser: Masers in the 1720-MHz ground-state satellite line are detectable in ∼6 per cent of 1665-MHz maser sources, with which they coincide to arcsecond accuracy (Caswell 1999). A brightness temperature $>10^{11}$ K has been estimated for W3(OH) (Masheder et al. 1994). 1720-MHz maser emission is also characteristic of supernova remnants.

In our calculations the 1720-MHz maser accompanies the 1665- and 1667-MHz emission, but appears under a more restricted range of conditions, for example requiring an OH specific column density $N_{OH}/\Delta V > 10^{10}$ cm^{-3} s. At high kinetic temperature the 1720-MHz maser is not evident except at low densities or very high dust temperatures. These model results are consistent with the 1720-MHz maser appearing only in 1665-MHz sources, and may be used to constrain the parameters describing sources in which the 1720-MHz maser is absent. We find the 1720-MHz maser to dominate the ground-state transitions at high values of $N_{OH}/\Delta V$, although this result depends on the reliability of our treatment of maser saturation.

1612-MHz $^2\Pi_{3/2}$ J = 3/2 F = 1–2 maser: Masers in the 1612-MHz ground-state satellite line are also detectable in ∼6 per cent of 1665-MHz maser sources, but almost always in the absence of 1720-MHz emission (Caswell 1999). Again, the 1612-MHz sources closely coincide with their 1665-MHz counterparts. Strong 1612-MHz maser emission is usually a feature of late-type stars.

We find the 1612-MHz maser to behave very differently from the other OH ground-state lines. It is complementary to the 1720-MHz transition, as noted by previous modellers, with one line commonly inverted while the other is in absorption. In our calculations the 1612-MHz maser appears in a zone of high density $n_H > 10^6$ cm^{-3}, high OH column density $N_{OH}/\Delta V > 10^{11}$ cm^{-3} s, and high gas temperature $T_k > 100$ K. Higher dust temperatures diminish the 1612-MHz maser, while lower dust temperatures enhance it. Since this line does not become a maser simultaneously with any of the other ground-state lines, the observations of 1612- and 1665-MHz masers in the same sources are not explained directly by common excitation conditions. Rather, we must hypothesize that the two masers are formed in nearby zones (as in models of late-type stars), with the rarer 1612-MHz masers flagging more extreme conditions in star-forming regions.

6035-MHz $^2\Pi_{3/2}$ J = 5/2 F = 3–3 maser: 6035-MHz main-line excited-state emission is detected at ∼30 per cent of 1665-MHz maser sites, with subarcsecond positional coincidence (Caswell 2001a). A few 6035-MHz maser sites have no detectable 1665-MHz emission (Caswell 1997). The 6035-MHz maser peak is generally weaker than its 1665 MHz counterpart (median ratio 5), although it is stronger in ∼10 per cent of cases (Caswell & Vaile 1995; Baudry et al. 1997; Caswell 1997, 2001a). The brightness temperature of the 6035-MHz maser exceeds 10^{10} K in W3(OH) (Desmurs et al. 1998). The majority of 1720-MHz maser sources also show emission at 6035 MHz (MacLeod 1997; Caswell 2001a).

This maser appears in a zone of low gas temperature, high density and high OH specific column density, partially coinciding with the 1665-MHz maser (Fig.1). The 6035-MHz maser is quenched at gas temperatures $T_k > 70$ K, while at lower gas temperatures it extends to density $n_H = 10^{8.5}$ cm^{-3}, requires OH specific column density $N_{OH}/\Delta V > 10^{10.3}$ cm^{-3} s, and is independent of dust temperature. The absence of this maser at low gas densities (Figs 1 and 2) indicates that collisions are involved in both generating and quenching the maser action. The prevalence of this maser in 1665-MHz sources suggests that low-temperature, high-density conditions are reasonably common, while the sites with 6035-MHz emission alone are likely to represent the high-density extreme. The coincidence with 1720-MHz maser sources is also naturally accounted for, but the illustrated calculations suggest that 1720-MHz emission should usually be detectable in sites hosting strong 1665- and 6035-MHz masers, whereas this is only sometimes observed.

6031-MHz $^2\Pi_{3/2}$ J = 5/2 F = 2–2 maser: Maser emission in the 6031-MHz excited-state main line is frequently present in 6035-MHz sources, although it is weaker and less often detected than at 6035 MHz (Baudry et al. 1997; Desmurs & Baudry 1998; Desmurs et al. 1998). There is a good match of positions between the 6031- and 6035-MHz lines in the few sources examined in detail (Desmurs & Baudry 1998; Desmurs et al. 1998; Caswell 2001a).

In our calculations the 6031-MHz maser closely accompanies the 6035-MHz maser, but is weaker by a small factor. Thus the close coincidence observed for these two lines is consistent with the modelling.

4765-MHz $^2\Pi_{1/2}$ J = 1/2 F = 1–0 maser: The dominant maser in the $^2\Pi_{1/2}$ ladder is in the 4765-MHz satellite line, with intensity up to 2 orders of magnitude weaker than the 1665-MHz ground-state emission (Szymczak, Kus & Hrynek 2000). 4765-MHz masers are found at sites hosting 6035-MHz masers and/or 1720-MHz masers (MacLeod 1997; Gray et al. 2001).

In the SD model this maser coincides to some extent with the $^2\Pi_{3/2}$ masers, but is less influenced by the situation in the ground state, and is the only transition to span the crossover between the 1612-MHz maser regime and that favouring the other masers (Figs 1, 2, 5 and 6). The 4765-MHz maser intensity increases with increasing dust temperature, and it is more apparent at higher gas temperature. This maser requires $N_{\rm OH}/\Delta V > 10^{10.9}\,{\rm cm}^{-3}\,{\rm s}$ to switch on, which is a higher threshold than the other masers apart from the 1612-MHz line (Fig. 1). The observed correlations with 1665-, 1720- and 6035-MHz masers are not strongly apparent in the results illustrated here, perhaps because this maser samples greater values of OH abundance than selected for Figs 2–7; this transition will be an important focus for future multitransition modelling.

3.3 Methanol–OH comparison

It has been shown that OH masers at 1665 MHz in star-forming regions coincide closely with methanol 6668-MHz masers (Caswell et al. 1995a,c, Caswell 1998). Most OH maser sites (~90 per cent) also host methanol masers, while OH masers are detected in approximately half of methanol maser sites (Caswell 1996). It is likely that masers in the two molecules form in close proximity, under similar excitation conditions, even if they do not form in precisely the same volume of gas. Our calculations allow the behaviour of the masers to be examined under identical model conditions, with the ratio of methanol to OH column density as an adjustable parameter. Figs 1–7 demonstrate that methanol and OH masers can appear simultaneously under a wide range of model conditions.

Methanol masers at 6668 MHz are usually observed to be stronger in flux density S than the 1665-MHz OH masers, and hence are more readily detected. Caswell (1996) finds that the methanol to OH intensity ratio $R = S(6668)/S(1665)$ extends continuously over a wide range with a typical value $R = 16$, and distinguishes the extreme source types: $R > 32$ are classified as methanol-favoured, $R < 8$ as OH-favoured, while the majority of sources lie in the range $8 < R < 32$.

In Figs 2–7 (bottom panel) the ratio of brightness temperatures in the dominant methanol and OH maser lines $T_{\rm b}(6668)/T_{\rm b}(1665)$ is plotted as a function of the model parameters. Since for a line of frequency ν emitting from a source of area Ω the flux density S is proportional to $T_{\rm b}\nu^2\Omega$, to compare the observed flux density ratio R with the model brightness temperature ratio requires an assumption about the relative size of the maser sources. If the methanol and OH maser spots are comparable in size, the typical flux density ratio $R = 16$ corresponds to a brightness temperature ratio of unity, since the frequency factor is $(6668/1665)^2 = 16$. Thus, under the assumption of equal maser source sizes, the typical source displaying both 6668-MHz methanol and 1665-MHz OH maser emission has approximately equal brightness temperatures in the two lines, while $T_{\rm b}(6668)/T_{\rm b}(1665) > 2$ in the methanol-favoured sources and <0.5 in the OH-favoured sources. Whatever assumption is made about relative spot sizes, the majority of the observations cluster over a narrow range of relative brightness temperatures.

The model values of the brightness temperature ratio $T_{\rm b}(6668)/T_{\rm b}(1665)$ vary over many orders of magnitude, reflecting exponential growth and sudden quenching of the masers. Ratios near 10^0 in Figs 1–7 are in accord with the typical observations, while values in the upper part of the plots represent strongly methanol-favoured ratios and values in the lower part of the plots represent strongly OH-favoured ratios. The ratio of brightness temperatures is determined by the choice of parameters $N_{\rm M}$ and $N_{\rm OH}$ (assuming equal maser linewidths ΔV for the two molecules). (Note that the ratio of column densities is actually $2N_{\rm M}/N_{\rm OH}$ because of the contributions from A and E methanol.) Fig. 3 (bottom panel) shows the brightness temperature ratio $T_{\rm b}(6668)/T_{\rm b}(1665)$ for three values of the ratio $N_{\rm M}/N_{\rm OH}$ at a low gas temperature. The maser brightness ratio is in the range 0.5–5 when $N_{\rm M}/N_{\rm OH} = 10$ for values of column density spanning 2 orders of magnitude. When $N_{\rm M} = N_{\rm OH}$ the OH maser turns on at lower column density, producing a strongly OH-favoured regime. At higher column density the methanol maser also turns on, giving brightness temperature ratios in the range 0.5–5 over about an order of magnitude range of column density, followed by a strongly methanol-favoured regime after the OH maser turns off. The reverse pattern occurs when $N_{\rm M}/N_{\rm OH} = 100$. When OH is more abundant with $N_{\rm M}/N_{\rm OH} = 0.1$, or when $N_{\rm M}/N_{\rm OH} = 1000$, the brightness temperature ratio switches between strongly OH-favoured and strongly methanol-favoured limits, since the OH and methanol masers are not present simultaneously.

The prevalence of model brightness temperature ratios in the range 0.5–5 is a result of both masers attaining peak brightness temperatures near 10^{11} K under the model conditions illustrated, with a tendency for the 6668-MHz maser to peak at a slightly higher value. This result is in excellent agreement with the observed ratios in the range 0.5–2 derived under the assumption of equal spot sizes. We suggest that the narrow range of observed flux density ratios is a result of both masers reaching a limit which is not strongly dependent on local conditions, as occurs when the masers become saturated. Our results are consistent with the observed flux ratio if the methanol maser spots are generally slightly smaller than the OH maser spots. However, the actual limiting value attained is determined by maser saturation, which is not particularly well modelled by our LVG treatment. A better treatment of maser saturation would generate more reliable peak brightness temperatures for these two strong masers, providing an estimate of the relative source sizes needed to replicate the observed flux density ratio.

We can conclude from Fig. 3 that the methanol column density parameter needs to be equal to or greater than its OH counterpart $1 < N_{\rm M}/N_{\rm OH} < 100$ if both masers are to become saturated simultaneously under a broad range of conditions. Limiting values $0.1 < N_{\rm M}/N_{\rm OH} < 1000$ apply to sources exhibiting maser action in both molecules. Ratios outside this range lead only to extreme cases where the favoured maser molecule is not just stronger, but is the only one detectable by many orders of magnitude. Methanol-favoured sources are not necessarily overabundant in methanol, however, as shown by the right-hand panel in Fig. 3, where the 6668-MHz methanol maser appears strongly in high-temperature sources (at high density and column density) in the absence of the OH 1665-MHz maser.

The ratio $N_{\rm M}/N_{\rm OH} = 10$ is illustrated in the remaining plots of $T_{\rm b}(6668)/T_{\rm b}(1665)$, since this gives broadest agreement with the observations, in that a common value of the brightness temperature ratio close to unity is derived from a variety of underlying conditions. The following conditions are seen to favour the 6668-MHz methanol maser: high kinetic temperature $T_{\rm k} > 125$ K with high gas density $10^{6.5} < n_{\rm H} < 10^8\,{\rm cm}^{-3}$ and dust temperature in the range $130 < T_{\rm d} < 230$ K. On the other hand, the 1665-MHz OH maser is favoured at low gas temperatures near the high-density limit $n_{\rm H} \sim 10^8\,{\rm cm}^{-3}$ and near the low dust temperature limit $T_{\rm d} \sim 100$ K, while at high gas temperatures the OH maser is

favoured in the low gas density / low specific column density part of the maser range (Fig. 4). Thus there are a variety of model conditions which can account for both the typical intensity ratios and the extremes observed.

For the excited state OH masers it was found that 6035-MHz maser positions are coextensive with methanol 6668-MHz masers at 29 sites harbouring both molecules and studied at subarcsecond resolution (Caswell 1997). Emission in the two molecules is also confined to the same velocity range. Some 74 per cent of 6035-MHz maser sites have 6668-MHz methanol maser counterparts (Caswell 2001a), with 1665-MHz maser emission also present in all but a few sources. These observations are consistent with the results of our modelling, in which the 6035-MHz masers appear in the low-temperature, high-density regime in which the methanol 6668-MHz maser is also present. The 6035-MHz masers extend to higher density than the methanol masers, so the sources in which 6035 and/or 1665-MHz OH emission is seen in the absence of methanol maser emission may represent densities $n_{\rm H} > 10^8\,{\rm cm}^{-3}$.

All 1720-MHz satellite-line maser sites studied also host methanol masers, but 1612-MHz masers do not coincide with methanol masers in half the sites studied (Caswell 1999). The 1720-MHz OH masers in our model occur only under conditions which also lead to the development of 6668-MHz methanol masers, so it is to be expected that they will coincide in sources with relative abundance $N_{\rm M}/N_{\rm OH}$ in the appropriate range. There is also some common ground between conditions favouring the 1612-MHz OH maser and the 6668-MHz methanol maser, although the former extends to higher gas density than the latter under high gas temperature conditions, and also extends to lower dust temperatures. An alternative possibility is that the methanol abundance is not usually sufficient to promote maser action under the warm gas conditions which favour the 1612-MHz maser. Low methanol abundance is presumably the reason for the absence of methanol masers in late-type stars, in which environment the 1612-MHz OH maser is dominant.

3.4 H II continuum emission

Infrared observations of maser sources in which the radio continuum from ionized gas is undetectable (Testi et al. 1994; Walsh et al. 2001) support the idea that the pumping conditions required for maser action can precede the development of an observable ucH II region. OH-favoured sites tend to have stronger ucH II counterparts than methanol-favoured sites (Caswell 1996, 1997, 2001a). Some 52 per cent of OH maser sites studied have associated ucH II regions (Forster & Caswell 2000). It is suggested that both OH and methanol masers signal recent high-mass star formation, switching off as the ucH II region progressively develops, with methanol masers both starting and finishing earlier, and thus tracing an earlier evolutionary stage.

In the SD model, continuum radiation from an underlying ucH II region is optionally included. The calculations presented in Figs 1–6 contain no ucH II spectrum, while Fig. 7 shows how this feature affects the maser brightness temperatures under selected model conditions. The effect of this radiation is to provide an additional source of low-frequency photons for amplification by the masers, while it is also implicated in the maser pumping via optical depth effects in the low-frequency lines. These two effects have opposing consequences for the maser intensities. The presence of a bright background can increase the maser brightness temperatures by up to three orders of magnitude if the H II region is sufficiently compact or distant from the maser site, as measured by the geometrical dilution factor $W_{\rm HII}$. When $W_{\rm HII} > 10^{-5}$, the H II emission starts to affect the level populations and reduces the optical depth of the masers, as shown in Fig. 7. The maser brightness is progressively reduced as $W_{\rm HII}$ is increased, eventually falling below the values obtained in the absence of any ucH II continuum (shown on the left of Fig. 7). The bottom panel of Fig. 7 shows that the OH masers are enhanced by a similar factor to the methanol masers for a very compact or distant underlying H II region, and the ratio of brightness temperatures in the methanol 6668-MHz and OH 1665-MHz lines is not sensitive to this additional feature. At our $T_{\rm k} = 30\,{\rm K}$ calculation point the brightness temperature ratio remains close to unity for the full range of $W_{\rm HII}$, while in the illustrated $T_{\rm k} = 150\,{\rm K}$ model the 1665-MHz OH maser is in absorption against the ucH II spectrum. Note that these results will be sensitive to the choice of turnover frequency ($f_{\rm e} = 12\,{\rm GHz}$) or emission measure of the ucH II region.

The peak brightness temperature attained is $\sim 10^{11}\,{\rm K}$ for both the methanol 6668-MHz and OH 1665-MHz masers for the calculations without the underlying ucH II continuum presented in Figs 1–6. VLBI observations suggest that the maser brightness temperatures may be even greater than this in some sources, e.g., $T_{\rm b} > 6 \times 10^{12}\,{\rm K}$ for 1665-MHz OH masers in 34.26+0.15 (Slysh et al. 2001) and $T_{\rm b} > 3 \times 10^{12}\,{\rm K}$ for 6668-MHz methanol masers in W3(OH) (Menten et al. 1992). Peak values greater than $10^{13}\,{\rm K}$ can be obtained from model calculations with larger beaming factors, or with a diluted H II background continuum as shown in Fig. 7.

4 DISCUSSION

The model calculations presented show that the observed close coincidence of OH and methanol masers in many sources has a natural explanation in terms of common excitation conditions which produce population inversions simultaneously in both molecules. The masers require infrared pumping radiation from warm dust ($T_{\rm d} > 100\,{\rm K}$). They are most likely to form in cooler gas ($T_{\rm k} < 100\,{\rm K}$) of moderately high density ($10^5 < n_{\rm H} < 10^{8.3}\,{\rm cm}^{-3}$), although higher temperatures and/or lower densities are also compatible with maser action. They are enhanced by beamed geometry and by the amplification of continuum photons from an underlying ucH II region. For both molecules the production of observable masers also requires an enriched gas-phase abundance to ensure sufficient optical depth.

Where masers from methanol and OH are observed to coincide closely, it is necessary that both be present at high abundance in the gas phase. Furthermore, it is likely that the masers in both molecules are generated under very similar excitation conditions. Our calculations show that there is a broad range of conditions which can satisfy these requirements. When, instead, masers of one or other molecule are seen in isolation, there are two possible explanations – either the non-masing molecule is not sufficiently abundant, or the local conditions produce maser action in the favoured molecule alone. Our calculations show that there is a very limited range of conditions which favour maser action in just one molecule. This means that the gas phase molecular abundance is probably the key determinant of methanol and OH maser activity in star-forming regions which produce the appropriate pumping environment.

Where 6-GHz methanol masers and 1665-MHz OH masers are both observed, the typical flux density ratio $8 < R < 32$ is matched by our model if the masers have similar spot sizes and both

approach the saturated limit. In this situation a range of temperature and density combinations give rise to similar values of R, consistent with the similar ratios observed in a variety of sources, with indications that methanol is likely to be more abundant than OH in the maser formation regions $2 < X_M/X_{OH} < 200$. This result needs to be confirmed by an improved treatment of maser saturation. While this seems to be the simplest explanation, it rests on several assumptions, and there are alternatives. The model can potentially account for the commonly observed flux ratio, even if the masers are weaker and unsaturated. However, this case sets much more stringent limits on the column densities of the two molecules, which must be closely correlated and in the narrow window where the maser brightness is rapidly rising (Fig. 3). Also, we have assumed that the masers in both molecules develop over the same path-length, but if the abundance enrichment of OH (say) is more localized, the path over which the methanol masers develop would be longer than that responsible for the OH masers, and our conclusions about relative abundance may be invalid. A further alternative is that the methanol maser spots are larger than the OH spots, producing a similar flux density in unresolved observations from a lower intrinsic brightness temperature.

Under our model assumptions the 6-GHz methanol maser approaches the saturated limit when $X_M > 10^{-6}$, while the 1665-MHz OH maser requires $X_{OH} > 10^{-7.3}$. Methanol favoured sources with $R > 32$ are likely to be overabundant in methanol but unsaturated in OH, so that $X_M/X_{OH} > 20$ while $X_{OH} < 10^{-7.3}$. Alternatively, they may be warm, dense sources ($T_k > 125$ K, $n_H \sim 10^7$ cm^{-3}) in which the 1665-MHz OH maser is inhibited but replaced by the 1612-MHz maser. The scarcity of 1612-MHz masers suggests that the OH abundance is usually $X_{OH} < 10^{-8}$ under these circumstances. OH-favoured sources with $R < 8$ are likely to be overabundant in OH but unsaturated in methanol, so that $X_M/X_{OH} < 20$ while $X_M < 10^{-6}$. Alternatively, they may be sources at the extremes of the maser range where the 6-GHz methanol maser is inhibited – e.g., cool sources near $n_H = 10^8$ cm^{-3} or $T_d = 100$ K, or warm sources near $n_H = 10^6$ cm^{-3}.

The weaker, less saturated, maser transitions are more sensitive to the physical conditions in the maser region, so that where several maser lines are observed in close coincidence, the presence or absence of particular lines can set limits on the temperature, density, etc. High-resolution studies are required to establish whether masers which appear to be close in position and velocity are really cospatial and propagating simultaneously through the same volume of gas. Such studies have not yet been undertaken for many sources at many frequencies. Meanwhile, multitransition modelling can investigate whether simultaneous maser pumping is a plausible explanation for the masers which appear to be closely associated, or whether a more sophisticated treatment involving gradients in certain properties will be required to explain the presence of several masers. In either case, upper limits on absent maser lines can set strong constraints on the local conditions.

Multitransition maser modelling has been undertaken for OH in W3(OH) (Cesaroni & Walmsley 1991; Gray et al. 1992), and for methanol in three sources (Cragg et al. 2001; Sutton et al. 2001). The wealth of data showing arcsecond positional coincidence for OH masers at different frequencies, and the statistics derived from surveys of many sources, invite a more general comparison with our model results. We find that the calculations presented here account for many, but not all, of the observed trends in OH. This may be because we have not yet sufficiently explored the vast parameter space. Note that the values of certain fixed model parameters were chosen from previous methanol maser modelling, so do not necessarily give the best agreement with the observations of OH. The OH masers may well be more sensitive than methanol to certain features of the modelling, as we found for line overlap, and future multitransition modelling of OH masers in selected sources will be valuable in refining the maser model. The fact that the SD model, developed for methanol masers, can reproduce so many of the OH maser trends lends strong support to the argument that masers in the two molecules coexist.

We find that the observed close coincidence of the 1665- and 1667-MHz masers is well explained by the SD model, while the prevalence of the weaker 1667-MHz masers suggests that the OH column density is usually in the range $10^{9.7} < N_{OH}/\Delta V < 10^{11.7}$ cm^{-3} s. The observed close coincidence between the 6035- and 6031-MHz masers is also a feature of the model, while the 30 per cent of sources in which these masers accompany the ground-state masers are expected to be low in temperature but high in gas density $10^6 < n_H < 10^{8.3}$ cm^{-3} and OH column density. Our model can readily explain observed coincidences between two or more of the 1665-, 1667-, 1720-, 4765-, 6035- and 6030-MHz masers in terms of simultaneous inversions; for example, all are inverted when $T_k = 30$ K, $10^{6.5} < n_H < 10^7$ cm^{-3}, and $10^{11} < N_{OH}/\Delta V < 10^{11.5}$ cm^{-3} s (Fig. 1). Among this group we would expect the least correlation between the 1667- and 4765-MHz masers because of their different OH column density requirements. A shortcoming in the illustrated results for OH is an overprediction of 1720-MHz masers, which are observed in a minority of sources displaying both 1665- and 6035-MHz masers, while in our calculations they are generally also present. Such observed trends can potentially set stringent limits on the model parameters describing the physical conditions in the maser regions. For example, a lower OH abundance and higher hydrogen density than we have selected can potentially account for such observations in sources in which the 1720-MHz maser is absent (Fig. 1). We also note that Masheder et al. (1994) found the 1720-MHz maser spot sizes to be considerably smaller than those at 1665 MHz. This means that the brightness temperatures which we model may correspond to lower 1720-MHz flux densities than predicted under the hypothesis of equal spot sizes. The 1612- and 1720-MHz masers are complementary in the modelling, consistent with their simultaneous appearance in very few sources. We find the 1612-MHz masers to be restricted to higher temperatures $T_k > 125$ K, again with high density and high OH column density, and the scarcity of these masers (6 per cent of sources) suggests that this combination of conditions is less common. In our calculations the 1612-MHz maser is accompanied only by the 4765-MHz maser, suggesting that the observed coincidences with other masers require a different explanation; for example, in the modelling of late-type stars the 1612-MHz masers and the main-line masers arise in shells experiencing different pumping conditions (Elitzur 1982).

The origin of the large gas-phase abundances of OH and methanol in maser regions is discussed in detail by Hartquist et al. (1995). Gas-phase chemical models do not produce sufficient methanol abundance except at temperatures >2000 K. On the other hand, there is evidence that methanol ice is highly abundant on grain mantles (e.g. Dartois et al. 1999). The hypothesis that the gas-phase methanol abundance is enriched in maser regions following the evaporation of icy grain mantles is supported by the observations of van der Tak, van Dishoeck & Caselli (2000). The dust is warmed ($T_d \sim 100$ K) following the development of a protostar, either by absorption of starlight or following the passage of a shock. The same process injects H_2O molecules into the gas phase,

with subsequent production of OH following photodissociation or ion–molecule chemistry. Thus it is quite plausible that methanol and OH should be simultaneously enriched in the gas phase as our maser model requires. Hartquist et al. argue that alternative mechanisms can produce enhanced OH abundance, but fail for methanol, so the observation of maser action in both molecules rules out these alternatives for star-forming regions.

The proposed evolutionary sequence is that methanol masers generally start and finish earlier than OH masers, but with a considerable time-span when both are present. Our maser modelling shows the critical effect of the molecular abundance; given sufficient abundance, masers appear in both molecules under the same conditions. This raises the possibility of tying the appearance of the masers to the evolution of the massive star via a 'chemical clock'. Several authors have modelled the gas-phase chemistry following the evaporation of grain mantles (reviewed by van Dishoeck & Blake 1998), although none to our knowledge has looked specifically at the methanol/OH abundance ratio.

Charnley, Tielens & Millar (1992) and Charnley et al. (1995) have investigated chemical models of hot cores in which grain mantle molecules are injected into the gas at time $t = 0$. The ensuing gas-phase ion–molecule chemistry is driven by cosmic ray ionization and the large methanol abundance. The gas temperature (100 K) and density ($10^{6.3}$–$10^{7.3}$ cm^{-3}) modelled are within our maser range. These models have methanol abundance $X_{\rm M} \simeq 10^{-6}$ out to $t = 10^4$ yr, dropping rapidly between $t = 10^5$ and 10^6 yr as the methanol is used up. The OH abundance is also enhanced as a result of injection of H_2O followed by protonation and dissociative recombination, and is strongly influenced by the oxygen chemistry (Charnley 1997). There is more OH at lower gas temperatures ($T_{\rm k} = 100$ K) than at higher gas temperatures ($T_{\rm k} = 300$ K) by some orders of magnitude as a result of temperature-dependent neutral–neutral reactions. At $T_{\rm k} = 100$ K the OH abundance peaks at $X_{\rm OH} \simeq 10^{-7.3}$ near $t = 10^5$ yr, before also dropping abruptly. The peak abundances of methanol and OH in these models are within the range we have identified as necessary for strong maser action, with the methanol abundance greater. It appears from these models that the OH abundance peaks after the methanol abundance has started to diminish. If confirmed by further chemical modelling, this would support the proposed evolutionary sequence outlined above. In this scenario the methanol masers appear after the evaporation of grain mantles, while the OH masers are more restricted to later times and lower gas temperatures where OH is efficiently produced, and masers in both molecules disappear after $\sim 10^5$ yr. We hope that these ideas will be further investigated by chemical models designed to study the evolution of the methanol/OH abundance ratio.

We have found that the presence of an underlying ucH II continuum source does not favour the pumping of OH masers over methanol masers. The greater correlation observed between OH maser and ucH II sites is therefore due to other factors, most likely related to the abundance of the maser molecules. Our results are consistent with the hypothesis that the methanol masers develop first if the methanol abundance peaks at an earlier time. The presence of a detectable ucH II region and the OH enrichment required for observable masers may be independent features of the later time development of the star-forming region. Alternatively, the OH masers may be a consequence of the ucH II region development if this leads to a greater rate of photodissociation of H_2O which further enhances the OH abundance.

Finally, we note that the gas-phase abundance also plays a key role in the development of masers in other environments. Methanol masers are known only in star-forming regions, where both class I and class II observations require enriched abundance. There are no methanol counterparts to the extragalactic OH megamasers (Phillips et al. 1998). We expect that OH masers occur in late-type stars, supernova remnants and in external galaxies in the absence of methanol masers, because these environments are conducive to the enrichment of OH alone.

5 CONCLUSIONS

The class II masers of methanol are found in close association with OH main-line masers in many regions of massive star formation, with some regions favouring methanol and some the hydroxyl masers. We have studied the pumping of these two maser molecules under identical model conditions for the first time. Masers of both molecules are pumped by IR radiation, and coexist over a wide range of model conditions. Our results strongly suggest that sources exhibiting maser action from only one molecule differ chemically from those with masers in both, since the same physical conditions promote maser action in both molecular species.

We find that line overlap does not contribute significantly to the maser pumping in methanol, whereas it is an essential feature of the OH excitation. Our treatment of OH masers employs the best available collisonal excitation rates, and sufficient energy levels to obtain reliable results for the excited state masers. Many features of the observed OH maser distribution are accounted for under these conditions, and multitransition fits will be useful for refining the model and identifying physical conditions in sources where several OH maser transitions are observed.

Assuming similar source sizes, the column density of methanol must be equal to or up to two orders of magnitude greater than that of OH to account for the typical production of 6668-MHz methanol masers and 1665-MHz OH masers at similar brightness temperatures. Our model suggests that these masers may be saturated. Sources in which the OH maser emission dominates are likely to have more moderate methanol abundance, while sources in which methanol maser emission dominates may be less rich in OH or with higher gas temperature conditions outside the 1665-MHz OH maser range.

The large gas-phase abundances of methanol and OH required for masers are thought to result from the evaporation of methanol and water ice from grain mantles. Since we have identified the abundance as a key determinant of maser activity for both molecules, modelling the evolution of the gas-phase methanol/OH ratio will help to tie the presence or absence of masers to the age of the emerging star.

ACKNOWLEDGMENTS

DMC and PDG acknowledge financial support from the Australian Research Council. AMS was supported by the Russian Federal Program 'Astronomy' and INTAS grant 97-11451.

REFERENCES

Argon A. L., Reid M. J., Menten K. M., 2000, ApJS, 129, 159
Baudry A., Desmurs J. F., Wilson T. L., Cohen R. J., 1997, A&A, 325, 255
Brown J. M., Schubert J. E., Evenson K. M., Radford H. E., 1982, ApJ, 258, 899
Castor J. I., 1970, MNRAS, 149, 111
Caswell J. L., 1996, MNRAS, 279, 79
Caswell J. L., 1997, MNRAS, 289, 203

Caswell J. L., 1998, MNRAS, 297, 215
Caswell J. L., 1999, MNRAS, 308, 683
Caswell J. L., 2001a, MNRAS, 326, 805
Caswell J. L., 2001b, in Migenes V., Lüdke E., eds, Proc. IAU Symp. 206, Cosmic Masers: from Protostars to Black Holes. Astron. Soc. Pac., San Francisco, in press
Caswell J. L., Haynes R. F., 1983, Aust. J. Phys., 36, 361
Caswell J. L., Haynes R. F., 1987, Aust. J. Phys., 40, 215
Caswell J. L., Vaile R. A., 1995, MNRAS, 273, 328
Caswell J. L., Vaile R. A., Ellingsen S. P., Whiteoak J. B., Norris R. P., 1995a, MNRAS, 272, 96
Caswell J. L., Vaile R. A., Ellingsen S. P., Norris R. P., 1995b, MNRAS, 274, 1126
Caswell J. L., Vaile R. A., Forster J. R., 1995c, MNRAS, 277, 210
Caswell J. L., Yi J., Booth R. S., Cragg D. M., 2000, MNRAS, 313, 599
Cesaroni R., Walmsley C. M., 1991, A&A, 241, 537
Charnley S. B., 1997, ApJ, 481, 396
Charnley S. B., Tielens A. G. G. M., Millar T. J., 1992, ApJ, 399, L71
Charnley S. B., Kress M. E., Tielens A. G. G. M., Millar T. J., 1995, ApJ, 448, 232
Codella C., Moscadelli L., 2000, A&A, 362, 723
Comben E. R., Brown J. M., 1988, Chem. Phys., 119, 443
Cragg D. M., Johns K. P., Godfrey P. D., Brown R. D., 1992, MNRAS, 259, 203
Cragg D. M., Sobolev A. M., Ellingsen S. P., Caswell J. L., Godfrey P. D., Salii S. V., Dodson R. G., 2001, MNRAS, 323, 939
Dartois E., Schutte W., Geballe T. R., Demyk K., Ehrenfreund P., d'Hendecourt L., 1999, A&A, 342, L32
Desmurs J. F., Baudry A., 1998, A&A, 340, 521
Desmurs J. F., Baudry A., Wilson T. L., Cohen R. J., Tofani G., 1998, A&A, 334, 1085
Destombes J. L., Marliere C., Baudry A., Brillet J., 1977, A&A, 60, 55
Elitzur M., 1982, Rev. Mod. Phys., 54, 1225
Ellingsen S. P., von Bibra M. L., McCulloch P. M., Norris R. P., Deshpande A. A., Phillips C. J., 1996, MNRAS, 280, 378
Field D., Gray M. D., 1988, MNRAS, 234, 353
Forster J. R., Caswell J. L., 2000, ApJ, 530, 371
Goorvitch D., Goldman A., Dothe H., Tipping R. H., Chackerian C., 1992, J. Geophys. Res., 97, 20771
Gray M. D., 2001, MNRAS, 324, 57
Gray M. D., Doel R. C., Field D., 1991, MNRAS, 252, 30
Gray M. D., Field D., Doel R. C., 1992, A&A, 262, 555
Gray M. D., Cohen R. J., Richards A. M. S., Yates J. A., Field D., 2001, MNRAS, 324, 643
Guilloteau S., Lucas R., Omont A., 1981, A&A, 97, 347
Hartquist T. W., Menten K. M., Lepp S., Dalgarno A., 1995, MNRAS, 272, 184
Lees R. M., Haque S. S., 1974, Can. J. Phys., 52, 2250
Liechti S., Wilson T. L., 1996, A&A, 314, 615
MacLeod G. C., 1997, MNRAS, 285, 635
Masheder M. R. W., Field D., Gray M. D., Migenes V., Cohen R. J., Booth R. S., 1994, A&A, 281, 871
Mehringer D. M., Zhou S., Dickel H. R., 1997, ApJ, 475, L57
Mekhtiev M. A., Godfrey P. D., Hougen J. T., 1999, J. Mol. Spec., 194, 171
Menten K. M., 1991, ApJ, 380, L75
Menten K. M., Reid M. J., Moran J. M., Wilson T. L., Johnston K. J., Batrla W., 1988, ApJ, 333, L83
Menten K. M., Reid M. J., Pratap P., Moran J. M., Wilson T. L., 1992, ApJ, 401, L39
Minier V., Conway J. E., Booth R. S., 2001, A&A, 369, 278
Moscadelli L., Menten K. M., Walmsley C. M., Reid M. J., 1999, ApJ, 519, 244
Norris R. P., Whiteoak J. B., Caswell J. L., Wieringa M. H., Gough R. G., 1993, ApJ, 412, 222
Offer A. R., van Hemert M. C., van Dishoeck E. F., 1994, J. Chem. Phys., 100, 362
Pavlakis K. G., Kylafis N. D., 1996a, ApJ, 467, 292
Pavlakis K. G., Kylafis N. D., 1996b, ApJ, 467, 300
Pavlakis K. G., Kylafis N. D., 1996c, ApJ, 467, 309
Pavlakis K. G., Kylafis N. D., 2000, ApJ, 534, 770
Peng R. S., Whiteoak J. B., 1993, MNRAS, 260, 529
Phillips C. J., Norris R. P., Ellingsen S. P., Rayner D. P., 1998, MNRAS, 294, 265
Reid M. J., Haschick A. D., Burke B. F., Moran J. M., Johnston K. J., Swenson G. W., 1980, ApJ, 239, 89
Röllig M., Kegel W. H., Mauersberger R., Doerr C., 1999, A&A, 343, 939
Slysh V. I., Kalenskii S. V., Val'tts I. E., 1995, ApJ, 442, 668
Slysh V. I., Kalenskii S. V., Val'tts I. E., Golubev V. V., Mead K., 1999, ApJS, 123, 515
Slysh V. I. et al., 2001, MNRAS, 320, 217
Sobolev A. M., Deguchi S., 1994a, A&A, 291, 569
Sobolev A. M., Deguchi S., 1994b, ApJ, 433, 719
Sobolev A. M., Cragg D. M., Godfrey P. D., 1997a, A&A, 324, 211 (SCG97a)
Sobolev A. M., Cragg D. M., Godfrey P. D., 1997b, MNRAS, 288, L39 (SCG97b)
Sutton E. C., Sobolev A. M., Ellingsen S. P., Cragg D. M., Mehringer D. M., Ostrovskii A. B., Godfrey P. D., 2001, ApJ, 554, 173
Szymczak M., Kus A. J., Hrynek G., 2000, MNRAS, 312, 211
Testi L., Felli M., Persi P., Roth M., 1994, A&A, 288, 634
Val'tts I. E., Dzura A. M., Kalenskii S. V., Slysh V. I., Booth R. S., Winnberg A., 1995, A&A, 294, 825
van der Tak F. F. S., van Dishoeck E. F., Caselli P., 2000, A&A, 361, 327
van Dishoeck E. F., Blake G. A., 1998, ARA&A, 36, 317
Walsh A. J., Hyland A. R., Robinson G., Burton M. G., 1997, MNRAS, 291, 261
Walsh A. J., Burton M. G., Hyland A. R., Robinson G., 1998, MNRAS, 301, 640
Walsh A. J., Bertoldi F., Burton M. G., Nikola T., 2001, MNRAS, 326, 36

This paper has been typeset from a TEX/LATEX file prepared by the author.